Journal of Physics: Conference Series

PAPER • OPEN ACCESS

Analysis of the Influence of Camber on Hydrodynamic Characteristics of Airfoil Based on FLUENT

To cite this article: Yang Yining 2020 *J. Phys.: Conf. Ser.* **1519** 012020

Analysis of the Influence of Camber on Hydrodynamic Characteristics of Airfoil Based on FLUENT

Yang Yining

Tianjin University, No.135 Yaguan Street, Tianjin Haihe Education Park, Jin'nan District, Tianjin, China

E-mail: 295171258@qq.com

Abstract. Based on hydraulic machinery blades airfoil design, numerical simulation was carried out for the hydrodynamics force of airfoil with different camber at Re=10^7. Firstly, the numerical simulation of airfoil was performed with structured grid and the Reynolds-averaged Navier-stokes-method, which coupled with the $k-\varepsilon$ turbulence model. Secondly, the drag and lift characteristics of airfoil with different camber were analysed. Finally, the flow field and pressure distribution of the airfoil was discussed. The result shows that as camber increases, drag, lift and lift-to-drag ratio increase, while the attack angle corresponding to maximum lift-to-drag ratio decreases. The results are useful for understanding the hydrodynamic performance of the airfoil, and provide an important theoretical basis for the design, selection and development of the airfoil in hydraulic machine.

1. Introduction

In the design of flow in hydraulic machinery, how to improve the hydrodynamic performance is one of the most important issues. As an important foundation for the design of power components of hydrodynamic machinery, the performance of airfoil has an enormous influence on hydrodynamic machinery. Therefore, the study on the performance of airfoil affects a lot on the development of hydrodynamic machinery. In recent decades, there has been many researches on the hydrodynamic characteristics of airfoil, both home and abroad. For example, Nowrouz Mohammad Nouri [1] et.al studied the effects of the camber ratio distribution over the blades of a NACA marine propeller. They found that the location of the maximum efficiency of the propeller is unchanged versus advance coefficient by changing the camber ratio over the blades. Li Rennian[1] studied the influence of airfoil camber of wind turbine on the aerodynamic performance of airfoil. Guo Junwu[3] studied the viscous flow around the airfoil blade of ship propeller. Xu Shixun [4] analysed the influence of airfoil on the gliding performance of gliders. M.A. Ashraf et.al studied the effect of varying airfoil thickness and camber on plunging and combined pitching and plunging airfoil propulsion [5]. Joel E. Guerrero [6] took a parametric numerical study to assess the effect of airfoil cambering on the aerodynamic performance of rigid heaving airfoil. The study shows that the airfoil cambering geometric parameter has a strong influence on the average lift coefficient, while it has a smaller impact on the average thrust coefficient and propulsive efficiency of heaving airfoil. A new concept of power generator using self-induced oscillating hydrofoil with upwind arm and downwind arm configurations to extract energy from fluid is proposed and numerically tested in the study of W. Jiang et.al [7]. Numerical results demonstrate that camber and critical pitching angle have significant effects on the energy

extraction performance of the power generator, and optimized camber and critical pitching angle configurations can increase the power coefficient and efficiency dramatically. The effects of large amplitude and no sinusoidal motion on pitching airfoil aerodynamics for thrust generation were numerically studied with a 2-D NACA0012 airfoil used, and various 2-D NACA asymmetric airfoil were applied for camber effect study [8]. The analytical solution for calculation of the unsteady air load on the airfoil with variable camber was derived for the incompressible potential flow [9]. The analytical solution for calculation of the unsteady air load on the airfoil with variable camber was derived for the incompressible potential flow [10].
In this paper, the numerical simulation of hydrodynamic characteristics of airfoil with different camber was carried out, and the influence of camber on hydrodynamic performance of airfoil was analysed, all by using the numerical simulation method, including the Reynolds N - S equation, the RNG $k-\varepsilon$ equation turbulence model and structured grids.

2. Governing equation

The flow around airfoil is incompressible flow. And the governing equations are two-dimensional incompressible n-s equations and two-dimensional continuity equations. The turbulent model is RNG $k-\varepsilon$ equations.

Two dimensional incompressible N-S equations:

$$\frac{\partial(\rho u)}{\partial t}+u\frac{\partial(\rho u)}{\partial x}+v\frac{\partial(\rho u)}{\partial y}=-\frac{\partial p}{\partial x}+\mu(\frac{\partial^2 u}{\partial^2 x}+\frac{\partial^2 u}{\partial^2 y}) \tag{1}$$

$$\frac{\partial(\rho v)}{\partial t}+u\frac{\partial(\rho v)}{\partial x}+v\frac{\partial(\rho v)}{\partial y}=-\frac{\partial p}{\partial y}+\mu(\frac{\partial^2 v}{\partial^2 x}+\frac{\partial^2 v}{\partial^2 y}) \tag{2}$$

RNG- $k-\varepsilon$ equations:

$$\frac{\partial(\rho k)}{\partial t}+\frac{\partial(\rho k u_i)}{\partial x_i}=\frac{\partial(\alpha_k\mu_{eff}\frac{\partial k}{\partial x_j})}{\partial x_i}+G_k+\rho\varepsilon \tag{3}$$

$$\frac{\partial(\rho\varepsilon)}{\partial t}+\frac{\partial(\rho\varepsilon u_i)}{\partial x_i}=\frac{\partial(\alpha_k\mu_{eff}\frac{\partial\varepsilon}{\partial x_j})}{\partial x_i}+\frac{C_{1\varepsilon}^*\varepsilon}{k}G_k-C_{2\varepsilon}\rho\frac{\varepsilon^2}{k} \tag{4}$$

$$\mu_{eff}=\mu+\mu_t;\mu_t=\frac{\rho C_\mu k^2}{\varepsilon} \tag{5}$$

$$C_{1\varepsilon}^*=C_{1\varepsilon}-\frac{\eta(1-\frac{\eta}{\eta_0})}{1+\beta\eta^3};\eta=(2E_{ij}E_{ij})^{\frac{1}{2}}\frac{k}{\varepsilon};E_{ij}=0.5(\frac{\partial u_i}{\partial x_j}+\frac{\partial u_j}{\partial x_i}) \tag{6}$$

3. Numeral calculations

3.1. Calculation model and grid generation

Considering full development of the flow and calculation convergence, the front and back boundary were taken 25 times the length of chord, while the upper and lower boundary were 32.5 times the length of chord.

Since the fluid field around the airfoil was relatively complex, grid around the airfoil surface needed to be set as intensive boundary layer grid.
For the computational domain, structured grids were used in this paper, and the total grids were 32724. The grids are shown in figure 1.

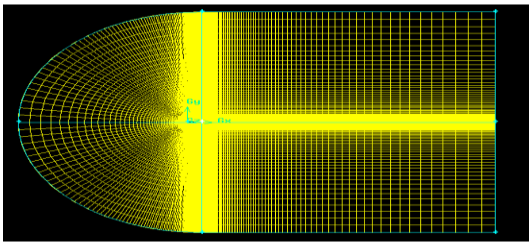

(a). Overall grids diagram

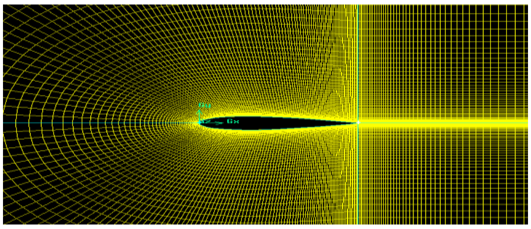

(b). Part of grids diagram

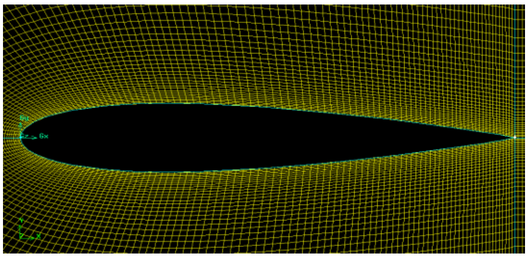

(c). Boundary layer grid

Figure 1. Calculation region and grids of airfoil NACA0415

3.2. Boundary conditions
(1). Inlet boundary conditions
The velocity inlet was set as the boundary condition of the inlet, and different attack angle was set with different velocity value and direction. The turbulent intensity of the inlet was 0.5, and the viscosity ratio was 5.
(2). Outlet boundary condition
The pressure outlet was adopted as the outlet boundary condition, and the other parameters were the same as the inlet.
(3). Wall boundary condition
No slip condition and no permeability condition were applied.
The above simulation method is verified in the reference [2].

4. Calculation results and analysis

In this paper, the Simple algorithm for calculation was adopted.
There are some important dynamic parameters of airfoil flow field calculation and analysis, including Reynolds number Re, drag coefficient C_d and lift coefficient C_L. They are defined as follows.
(1) Reynolds number. Dimensionless parameter characterizing inertial force and viscous force: $Re = \rho VD/\mu$, where V is the velocity of incoming flow; D is the characteristic length of airfoil. In this paper, the Reynolds number is 10^7.

(2) Drag coefficient C_d. Airfoil drag consists of surface friction and boundary layer's differential pressure. The typical airfoil drag F_d is characterized by the airfoil drag coefficient C_d: $C_d = F_d/ (\rho V^2 D/2)$

(3) Lift coefficient C_L. Dimensionless, it is the ratio of lift to the product of hydrodynamic pressure and reference area of the airfoil. $C_L = F_L/ (\rho V^2 D/2)$. In the calculation, F_L is lift.

In this paper, naca0415, naca2415, naca4415, naca6415 and naca8415 with a chord length of 1m were taken as the original airfoil.

Under the condition of the same relative thickness of airfoil, relative position of the maximum thickness and position of the maximum camber, numerical simulation were conducted on the above airfoil with different maximum relative curvature f_{max}/l of 0, 2%, 4%, 6%, 8%. The attack angle was 0°-14°with 2 ° interval.

4.1. Lift and drag coefficients

According to the numerical calculation results, for the airfoil whose maximum relative camber was 2%, the variation of airfoil's drag and lift coefficient with the attack angle is shown in figure 2 and figure 3.

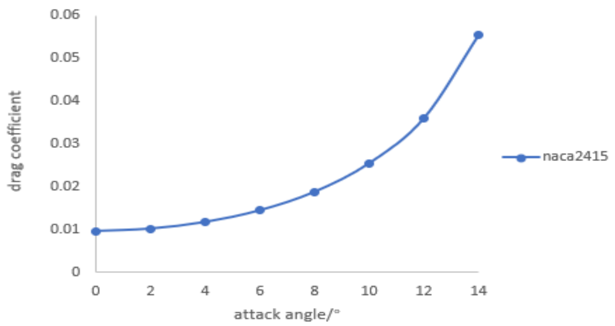

Figure 2. Curve of airfoil's drag coefficient with the variation of attack angle

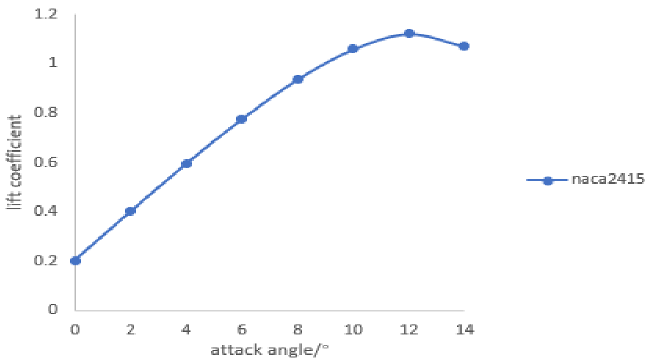

Figure 3. Curve of airfoil's lift coefficient with the variation of attack angle

It can be seen from figure 2 and figure 3 that with the increase of the attack angle of incoming flow, airfoil's lift/drag coefficient increase gradually. When attack angle is between 0°-12°, the lift coefficient presents a linear change, while the drag coefficient presents a parabolic change. When attack angle is larger than 12°, the lift coefficient starts to decrease, while the drag coefficient has a tremendous increase. This is because that airfoil is in a state of stall at a large attack angle. With attack angle keeping increasing, the separation degree of airfoil flow is aggravated and airfoil goes into a state of deep stall.

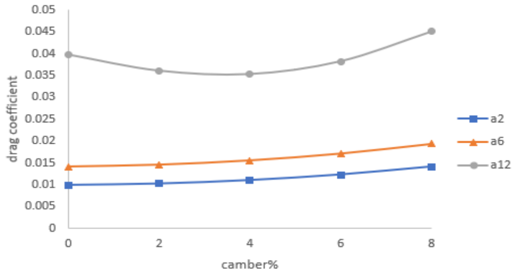

Figure 4. Curves of airfoil's drag coefficient with different camber

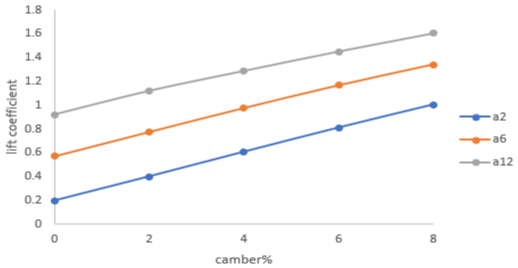

Figure 5. Curves of airfoil's lift/drag coefficient with different camber

Figure 4 and Figure 5 show curves of airfoil's drag/lift coefficient with different camber.
It can be seen from figure 4 that with the increase of camber, the drag coefficient of airfoil increases uniformly at a small attack angle. However, with the increase of camber at a large attack angle, the drag coefficient first decreases and then increases. It can be seen from figure 5 that lift coefficient of airfoil increases linearly with the increase of camber.

4.2.Lift-to-drag ratio
Figure 6 shows the relation curves of lift-to-drag ratio at attack angles of 0°, 2°, 10° and 12°. Figure 7 shows the variation trend of lift-to-drag ratio with attack angles of airfoil with different camber.

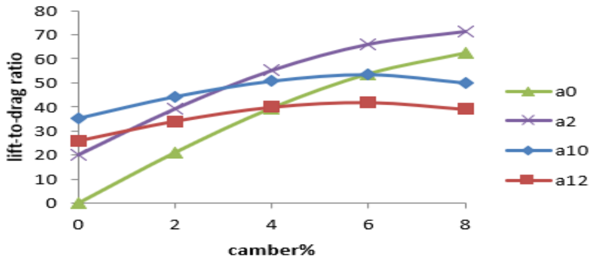

Figure 6. The relation curve of lift-to-drag ratio with camber

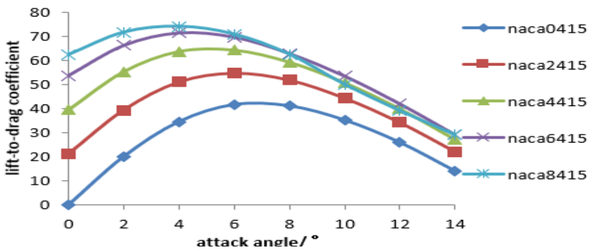

Figure 7. The relation curve of lift-to-drag ratio with attack angle

It can be seen from figure 6, when the attack angle is small (such as 0° and 2°), the lift-to-drag ratio increases with the airfoil camber increases. When the attack angle is large (such as 10° and 12°), the lift-to-drag ratio first increases and then decreases as the camber increases. When the camber reaches 6%, the lift-to-drag ratio starts to decrease. It can be seen that if other conditions are not changed, the dynamic performance of the airfoil could be effectively improved by appropriately increasing the airfoil camber.

It can be seen from figure 7 that the lift-to-drag ratio of the same airfoil will first increase and then decrease with the increase of attack angle of the incoming flow. The best attack angle and the maximum lift-to-drag ratio of airfoil with different camber are different. For slightly curved airfoil, the maximum lift-to-drag ratio appears at 6°- 8° attack angle. With the increase of camber, the attack angle corresponding to the maximum lift-to-drag ratio decreases. For naca8415, the maximum lift-to-drag ratio appears at 4° attack angle.

Five airfoil's lift-to-drag ratios with different attack angles were obtained in this research.

Table 1 shows the maximum lift-to-drag ratio of airfoil and its corresponding lift/drag coefficients and best attack angle. The design of camber and attack angle of the selected airfoil can be preliminarily determined according to the calculation results in practical application.

Table 1. The maximum lift-to-drag ratio of airfoil and its corresponding coefficients

camber	best attack angle	drag	lift	lift-to-drag ratio
0	6	0.0140	0.5719	40.5876
2	6	0.0145	0.7758	53.4045
4	4	0.0127	0.8017	63.0327
6	4	0.0141	1.0025	70.6561
8	4	0.0162	1.1884	73.1036

4.3. Analysis of flow field

Pressure distribution and X velocity distribution of airfoil with 0%, 4%, 8% camber at 6°, 4° and 4° attack angles corresponding to their maximum lift-to-drag coefficient are shown in Figure 8 and 9.

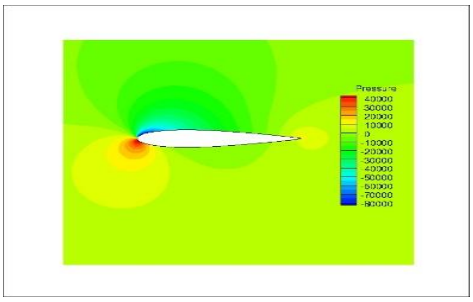

(a). Pressure distribution of naca0415 at 6° attack angle

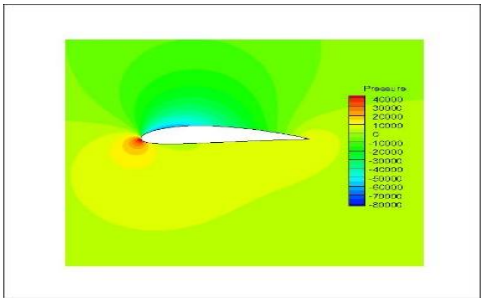

(b). Pressure distribution of naca4415 at 4° attack angle

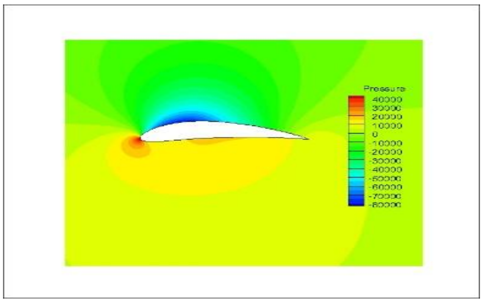

(c). Pressure distribution of naca8415 at 4 °attack angle
Figure 8. Pressure distribution

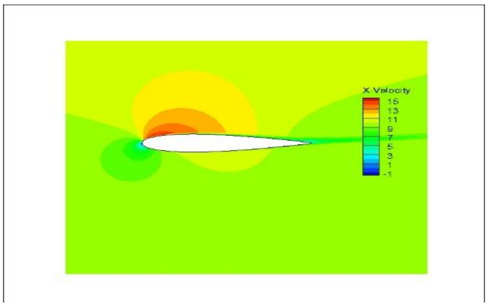

(a). X velocity distribution of naca0415 at 6 °attack angle

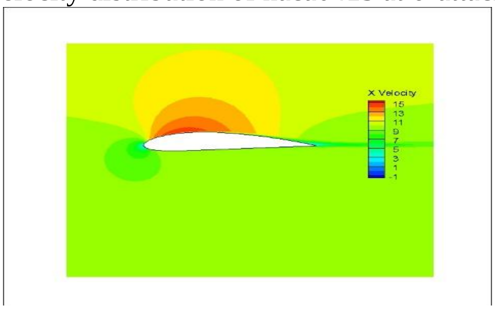

(b). X velocity distribution of naca4415 at 4 °attack angle

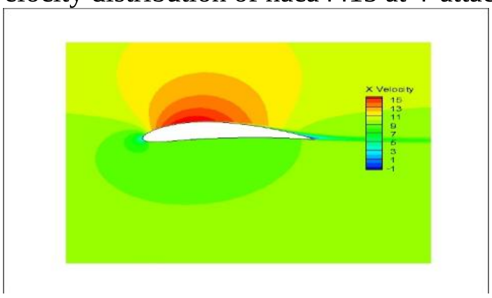

(c). X velocity distribution of naca8415 at 4 °attack angle
Figure 9. X velocity distribution

Figure 8 and Figure 9 show that point of high pressure is always at the airfoil head because of the impact of the incoming flow, and that of low pressure always appears on upper surface.
With the increase of camber, the region of the low pressure on upper surface moves backward due to streamlines on the upper surface gathering. Therefore, with the increase of camber, the low pressure on the airfoil’s upper surface decreases, and the high pressure on the lower surface increases. As a result, the pressure difference of the airfoil increases. In addition, with the increase of camber, the flow velocity of the upper surface raises, and the area vertical to the incoming flow becomes lager, which can lead to the increase of airfoil drag.

4.4. Pressure distribution

The lift of airfoil is generated by the difference of pressure between the upper and lower surfaces. Usually, the contribution of the low pressure on the upper surface to the lift is much greater than the high pressure on the lower surface, and the lowest pressure occurs near the head of the upper surface, where cavitation bubbles often occur. Figure10 shows the curves of pressure distribution on upper and lower surfaces when the airfoil's camber is 0, 4% and 8% and at best attack angles.

As shown in Figure 10, with the increase of camber, the pressure on the lower surface of the airfoil becomes lower while the pressure on the upper surface becomes higher, thus increasing the pressure difference between the upper and lower surfaces. The pressure distribution of the upper and lower surfaces also changes obviously. The main area of the pressure difference changes from the head to the middle of airfoil, and the area where the lowest pressure occurs on the upper surface also moves from the head to the middle of airfoil, where the relative chord length is about 3%, 12% and 22%.This is because that with the increase of camber, the arch degree of the upper surface is the largest in the area with relative chord length of about 3%, 12% and 22%, where the streamline extrudes, velocity increases and pressure decreases; While the area where the highest pressure occurs on the lower surface also moves from the head to the middle area of the airfoil.

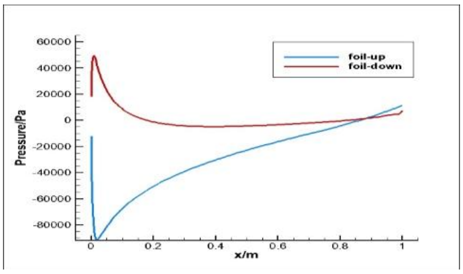

(a). Curves of pressure distribution on upper and lower surfaces of naca0415 at 6 °attack angle

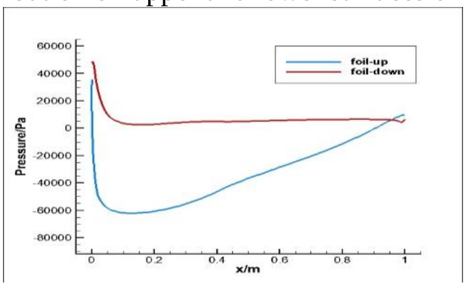

(b). Curves of pressure distribution on upper and lower surfaces of naca4415 at 4 °attack angle

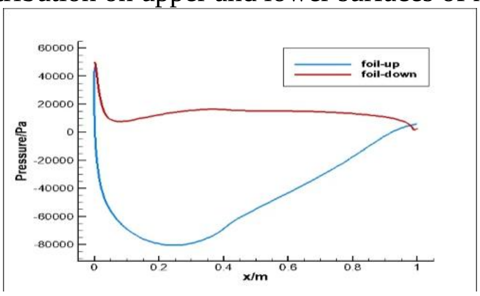

(c). Curves of pressure distribution on upper and lower surfaces of naca8415 at 4 °attack angle

Figure 10. Curves of pressure distribution on upper and lower surfaces

5. Conclusion

In the present work, the effect of camber on hydrodynamic performance of nacaX415 airfoil was assessed. Standard $k-\varepsilon$ model and SIMPLE algorithm were adopted. Lift/Drag coefficient, lift-to-

drag ratio, velocity and pressure distribution on the surface of airfoil with different camber at different attack angles were analysed. The conclusions are as follows:
(1). With the increase of airfoil's camber, the pressure difference between the upper and lower surfaces increases, which means lift increases greatly amplitude. Meanwhile, drag also increases, but the growth is smaller than that of lift. Therefore, in order to improve the hydrodynamic performance of airfoil, the change of lift-to-drag ratio should be considered. It is concluded that the lift-to-drag ratio increases with the increase of camber in a certain range, first increases and then decreases with the increase of attack angle. In this paper, the maximum lift-to-drag ratio of airfoil was obtained under limited conditions.
(2). With the increase of airfoil's camber, the distribution of negative pressure on the upper surface gradually moves from the head to the middle part of the airfoil. However, cavitation firstly appeared here in the case of large attack angle, which should be considered in the actual design.
(3). In the numerical simulation of airfoils with different camber, the influence of camber on airfoil's performance was only considered, while other factors were not taken into consideration. Airfoil's performance is affected by the overall geometry, such as camber, relative thickness, position of maximum relative thickness and position of maximum camber. However, camber has a greater influence on it. Therefore, in order to improve the hydrodynamic performance of airfoil, other influencing factors and cavitation should be considered comprehensively.

References

[1] Nowrouz Mohammad Nouri , Saber Mohammadi, Numerical investigation of the effects of camber ratio on the hydrodynamic performance of a marine propeller[J].Ocean Engineering, 2018(148):632-636.
[2] Li Rennian, Zhang Shiang, Yang Rui, Li Shunde. Influence of airfoil camber of wind turbine on aerodynamic performance of wind airfoil [J]. Fluid machinery, 2009,37(5): 17-21.
[3] Guo Junwu, Zhang Huaixin, Research on the viscous flow around the airfoil blade of ship propeller [J]. Ship engineering, 2014,36(6): 31-33.
[4] Xu Shixun, Liu Yuhong, Zhu Yaqiang, Wang Yanhui. Analysis on the influence of airfoil on glider gliding performance [J]. China mechanical engineering, 2017,28(3): 286-293.
[5] M.A. Ashraf, J. Young, J.C.S. Lai. Reynolds number, thickness and camber effects on flapping airfoil propulsion[J]. Journal of Fluids and Structures,2010,27(2).
[6] Joel E. Guerrero. Effect of Cambering on the Aerodynamic Performance of Heaving Airfoils[J]. Journal of Bionic Engineering,2009,6(04):398-404+406-407.
[7] W. Jiang,D. Zhang,Y.H. Xie. Numerical investigation into the effects of arm motion and camber on a self-induced oscillating hydrofoil[J]. Energy,2016,115.
[8] K. Lu,Y.H. Xie,D. Zhang. Numerical study of large amplitude, nonsinusoidal motion and camber effects on pitching airfoil propulsion[J]. Journal of Fluids and Structures,2013,36.
[9] Mihael Mesarič,Franc Kosel. Unsteady airload of an airfoil with variable camber[J]. Aerospace Science and Technology,2003,8(3).
[10] Mihael Mesarič,Franc Kosel. Unsteady airload of an airfoil with variable camber[J]. Aerospace Science and Technology,2003,8(3).